IJE TRANSACTIONS B: Applications Vol. 39, No. 08, (August 2026) 1829-1842

International Journal of Engineering

Journal Homepage: www.ije.ir

Behavior of a Next-Generation Nickel Super Alloy Turbine Component under Direct Exposure to Gas Heat from Combustion in a Long-term Operation

A. Faraji[a], M. R. Rahimipour*[a], M. Farvizi[b], H. Omidvar[c]

[a] *Ceramic Division, Materials and Energy Research Center, Karaj, Iran*
[b] *Department of Materials Engineering, Faculty of Mechanical Engineering, University of Tabriz, Tabriz, Iran*
[c] *Department of Mining and Metallurgical Engineering, Amirkabir University of Technology (Tehran Polytechnic), Tehran, Iran*

PAPER INFO

Paper history:
Received 02 August 2025
Received in revised form 20 September 2025
Accepted 28 September 2025

Keywords:
Nickel Superalloy
Carbides and γ′ - Phase Metallographic Evaluation
MAUD
XRD
Creep Resistance

ABSTRACT

In this research, the microstructural evolution and creep behavior of a second-stage vane from a gas turbine after 1200 long-term cycles were evaluated through microstructural examinations and creep tests. Microscopic analyses revealed an increase in the volume fraction and size of secondary phases such as gamma prime and carbides. These microstructural changes led to the embrittlement of the investigated nickel superalloy. Hardness testing results indicated an increase in hardness from 420 Vickers to 480 Vickers for the service-exposed vane after direct exposure to gas heat. Thermal analysis showed a 60°C decrease in the complete dissolution temperature, suggesting a need for repair or rejuvenation of the alloy. The growth of gamma prime precipitates through the shearing of dislocations and the coarsening of carbides due to the inhibition of grain boundary sliding resulted in an 11-hour reduction in creep life. The reference sample failed at a stress of 247 MPa and a temperature of 900°C after 40 hours with a strain of 9%. In contrast, the service-exposed vane exhibited a reduction in creep life and creep strain to 29 hours and 4%, respectively.

doi: *10.5829/ije.2026.39.08b.05*

Graphical Abstract

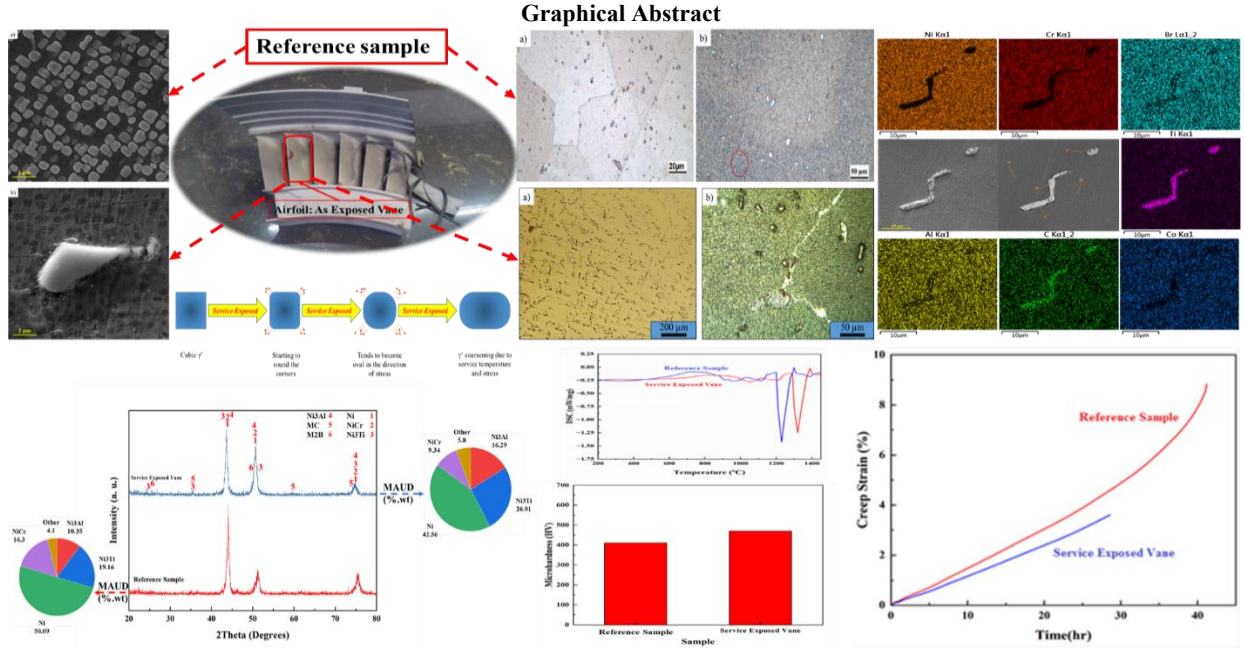

*Corresponding Author Email: m.rahimipour@merc.ac.ir (M. R. Rahimipour)

Please cite this article as: Faraji A, Rahimipour MR, Farvizi M, Omidvar H. Behavior of a Next-Generation Nickel Super Alloy Turbine Component under Direct Exposure to Gas Heat from Combustion in a Long-term Operation. International Journal of Engineering, Transactions B: Applications. 2026;39(08):1829-42.

1. INTRODUCTION

Nickel-based superalloys have found indispensable applications, particularly in aerospace and high-temperature environments such as turbine blades (1). The continuous pursuit of higher operating temperatures and improved performance in gas turbines has driven the development of these advanced materials. However, the service life of these alloys is significantly compromized by various factors including creep, fatigue, erosion, hot corrosion, and oxidation. These degradation mechanisms often interact synergistically, accelerating the deterioration process (2-5). Furthermore, microstructural evolution induced by severe service conditions such as high temperature and stress plays a crucial role in the degradation of these components (6). Next-generation nickel-based superalloys are widely used in the manufacturing of turbine blades and vanes (7-9). Their exceptional high-temperature properties make them suitable for challenging applications in the hot section components of turbines (8). However, prolonged exposure to harsh operational conditions can lead to the degradation of mechanical properties. To mitigate these challenges, ongoing research is focused on developing advanced superalloys such as the oxidation-resistant TMS-238 with improved performance characteristics (10). Previous research has extensively investigated the behavior of nickel superalloys. Tyagunov et al. (11) observed the formation of carbides and brittle phases in ZhS6U superalloy during prolonged exposure to high temperatures. Furthermore, studies by Tewari et al. (12) examined the impact of alloying modifications in ZhS6K superalloy, indicating that B/C modifications can enhance yield strength while potentially reducing ductility and tensile fracture properties. These previous investigations on ZhS6U and ZhS6K superalloys, which are pertinent to the broader family of nickel-based superalloys, provide a foundational understanding for evaluating the behavior of a next-generation nickel superalloy turbine component under direct exposure to gas heat from combustion in long-term operation, as explored in the present study. Addition of boron can significantly alter the microstructure and mechanical properties of the investigated nickel superalloy. The microstructure of nickel-based superalloys plays a crucial role in determining their mechanical behavior. In solid-solution alloys, larger crystal grain sizes can lead to abnormal grain growth, resulting in reduced strength and fatigue resistance (5, 13). Moreover, grain boundary diffusion facilitates the diffusion of chromium (Cr) and carbon (C), depleting the matrix and compromising the formation of protective oxide layers (14-19). Such phenomena has increased susceptibility to hot corrosion, oxidation, and intergranular fracture significantly impacts alloy performance. In precipitation-hardened alloys, such as ZhS-family superalloys, the microstructural variations during working conditions become more complex. The size, distribution, and morphology of precipitates, such as gamma prime (γ'), significantly influence creep resistance. Coarsening of γ' precipitates weakens the alloy by facilitating dislocation motion and leading to reduced creep resistance (2, 6, 20-26). The formation of other detrimental phases, such as delta, sigma, and mu, can create lattice mismatches and initiate and accelerate crack propagation (16, 27). Additionally, the formation of chromium-stabilized secondary carbides at grain boundaries can deplete the matrix and promote γ' precipitate growth, which can lead to the formation of creep voids and accelerated microstructural degradation. The microstructural features of Ni-based superalloys, including the solid solution (γ phase), primary carbides (MC type), and intermetallic precipitates ($Ni_3(Al, Ti) - \gamma'$), significantly influence their mechanical properties (9). Larger precipitates and carbides can lead to reduced creep rupture life and increased fatigue crack initiation (9). While the presence of the γ' phase generally improves mechanical properties, its impact can vary depending on the alloy composition and specific microstructure. For instance, in a specific single-crystal nickel-based superalloy, the presence of the γ' phase had no significant impact on mechanical properties (28). Furthermore, undesirable microstructural features, such as segregation of alloying elements, can significantly compromise the desired properties. For instance, in Ni-Cr-Al-Ti alloys processed by laser powder bed fusion, segregation of solute elements to grain boundaries during processing can significantly affect consolidation behavior (29, 30).

Turbine blades and vanes are critical components in gas turbines. The microstructure of nickel-based superalloys plays a crucial role in determining their mechanical behavior. High-performance turbine components are typically manufactured from precipitation-strengthened nickel-based superalloys, which derive their exceptional high-temperature strength and creep resistance primarily from the controlled precipitation of ordered intermetallic phases, notably the γ' phase.

The relatively constant high-temperature environment prevailing in certain critical stages of a gas turbine, such as those exposed to sustained elevated temperatures, can accelerate microstructural changes in the vanes, leading to embrittlement and reduced resistance to impact, wear, and fatigue. This degradation can ultimately result in creep and premature failure of these critical components. It is significant to delve deeper into the changes that occur after long-term operations of expensive and critical parts in a gas turbine. Given the practicality of advanced single-crystal nickel-based superalloys, such as CMSX-4, it is very important to investigate their behavior quantitatively and qualitatively due to direct exposure to combustion chamber exhaust

gas. CMSX-4, as a prominent example of next-generation superalloys, is characterized by its high refractory element content and precise gamma prime phase morphology, which contribute to its superior high-temperature strength and creep resistance.

While the degradation behavior of nickel-based superalloys has been extensively investigated in the literature, the majority of these studies have primarily focused on laboratory-scale, accelerated aging tests conducted on pristine materials. Such controlled experiments are valuable for understanding basic material behavior, they often fail to replicate the complex and synergistic effects of real-world service environments, which involve long-term thermal cycles, varying mechanical loads, and direct exposure to high-temperature combustion gases. As a result, these studies may not fully capture the material degradation that occurs under the actual operating conditions encountered in service environments.

The innovation of our study lies in its focus on a real-world turbine vane made from a next-generation nickel superalloy (CMSX-4), which has undergone 1200 hours of long-term service in an operational gas turbine. This allows us to provide a unique and authentic dataset on the degradation mechanisms that occur under true operational conditions. Specifically, our research offers a novel contribution in the following ways:

1. **Investigation of a Realistic Degradation Profile:** Unlike prior studies that typically focus on simplified laboratory conditions, our research analyzes the response of a full-scale turbine component to the complex combination of thermal cycling, mechanical stresses, and direct exposure to combustion gases. We have identified distinct degradation patterns between the hot-gas-exposed region and the trailing edge, which has been subjected to significantly different thermal histories. This nuanced degradation profile, which is directly relevant to service environments, is rarely captured in laboratory-based studies.
2. **Multi-Scale Characterization and Cause-and-Effect Relationship:** Our study employs a comprehensive suite of advanced characterization techniques, including optical microscopy (OM), field-emission scanning electron microscopy (FESEM/EDS), X-ray diffraction (XRD/Rietveld analysis), differential scanning calorimetry (DSC), hardness testing, and creep testing. Through this multi-technique approach, we have established a direct cause-and-effect relationship between the observed microstructural evolution (e.g., γ' phase dissolution and carbide coarsening) and the corresponding changes in mechanical properties, including creep resistance. This level of multi-scale analysis provides a more detailed and confident understanding of the degradation mechanisms, surpassing the scope of previous studies that often relied on fewer or less comprehensive methods.
3. **Real-World Implications for Turbine Component Longevity:** By studying a turbine component subjected to real-world operational conditions, our work bridges the gap between fundamental materials science and practical engineering applications. We provide crucial insights into the material's performance under service conditions, which is essential for predicting the longevity and reliability of turbine components. This research not only advances our understanding of the material degradation processes but also contributes valuable data to the development of more reliable turbine components and better maintenance strategies.

2. EXPERIMENTAL

This study investigated a turbine vane that had undergone approximately 1200 operational cycles during its service life. Each cycle simulated real-world gas turbine conditions involving thermal and mechanical loading. During each cycle, the turbine vane was heated to a peak temperature of approximately 1000 °C. The vane was held at this peak temperature for around 1200 hours, corresponding to the steady-state operation phase of the engine. Following this hold period, the component experienced a controlled cooling stage with a gradual temperature decrease during flight. The cooling was completed by a rapid quench during engine shutdown, which contributed to thermal gradients within the material. In addition to thermal cycling, the turbine vane was subjected to significant mechanical stresses throughout its operation. These stresses originated from centripetal forces due to high-speed rotation and from gas pressure loads within the turbine. The simultaneous exposure to elevated temperature and mechanical loading imposed complex thermo-mechanical conditions on the component, which are fundamentally different from those encountered in typical laboratory tests. The cumulative effect of these thermal and mechanical cycles led to microstructural changes in the turbine vane, including γ′ phase dissolution and carbide morphology evolution. These phenomena were investigated to understand the long-term degradation behavior under realistic service conditions. Figure 1 shows an image of the turbine vane before service exposure (reference sample) and after exposure to service. As observed in Figure 1, a significant portion of the initial coating on these vanes has degraded during service operation. In the initial phase of this study, the chemical composition of the turbine vane and the reference sample was analyzed using optical emission spectroscopy. This analysis

revealed that the turbine vane was fabricated from a nickel-based superalloy known as a next-generation nickel superalloy. Table 1 presents the weight percentage of the selected components.

Phase analysis of the investigated nickel superalloy was conducted using a Siemens D-500 X-ray diffractometer. The XRD analysis employed Cu Kα radiation with a voltage of 20 kV, a wavelength of λ=0.154 nm, and a current of 30 mA. For microstructural characterization, samples were cut from the service-exposed turbine vane and the reference sample. Microstructural studies were carried out using an Olympus optical microscope and a TESCAN MIRA3 field emission scanning electron microscope (FESEM) equipped with an energy-dispersive X-ray spectroscopy (EDS) system, both manufactured by Czech Republic.

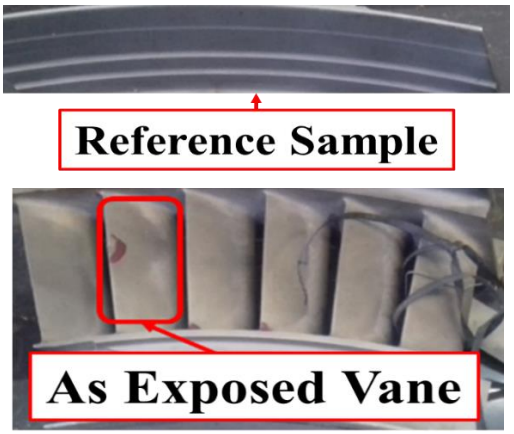

Figure 1. Reference sample and service-exposed turbine vane

TABLE 1. Chemical composition of both the reference sample and service-exposed vane was determined in terms of weight percentage

Elements	Ni	C	Cr	Co	Mo	Al	Ti	Si	Fe	Re	Ta	B	W	Hf
Reference Sample	Base	0.07	6.80	9.40	0.75	5.29	1.52	0.03	0.11	2.91	6.66	0.01	6.70	0.11
Service Exposed Vane	Base	0.06	6.35	8.91	0.60	5.25	1.16	0.01	0.17	2.92	6.55	0.01	6.65	0.95

Prior to analysis, samples were meticulously polished with sandpaper up to 3500 grit and then subjected to microetching on the damaged sample according to the ASTM E404-2015 standard, and electropolishing for the undamaged sample. The etching solution consisted of 170 ml phosphoric acid, 10 ml sulfuric acid, and 16 g CrO_3. Samples were electropolished in this solution at 5 volts for 5-7 seconds (20, 31, 32). Hardness measurements were conducted using the Vickers method, with an average of five indentations recorded for each sample. Rietveld refinement analysis was employed to accurately calculate the weight percentage and determine the crystallographic information of the present phases. This analysis was performed using the MAUD software. The quality of the Rietveld refinement was evaluated based on the "sigma" and "R" factors. Throughout the Rietveld analysis in this study, the sigma and R values were consistently below 2 and 10, respectively, indicating the reliability of the quantitative analysis. Additionally, all peaks were effectively covered by the CIF cards of different phases. In summary, the combination of XRD, SEM, EDS, and Rietveld refinement analyses provided comprehensive insights into the phase composition and structural features of the sample. To determine the temperature at which liquid formation occurs, the initial melting temperature of the phases was investigated using differential scanning calorimetry (DSC) with a Netzsch STA449 F3 Jupiter device in an argon environment. The sample was heated at a rate of 20 °C/min up to 1500 °C. The sub-size creep tests were conducted using a SANTAM STM-20M2 creep testing machine under constant uniaxial tensile stress conditions. The test temperature was maintained at 900°C, and a constant stress of 247 MPa was applied throughout the experiments. These conditions were carefully selected to simulate the high-temperature mechanical environment typically experienced by turbine vanes during service. The creep specimens were extracted from both the service-exposed turbine vane and the reference material, and all samples were prepared using consistent machining and surface finishing procedures to ensure the reliability of the comparison. The specimens were designed and machined in accordance with the specifications for sub-size specimens as per ASTM E139 standard, with a gauge length of 25 mm and a gauge diameter of 5 mm.

3. RESULTS AND DISCUSSION

Figure 2 presents OM images of the microstructure in the referenve sample of the vane, which was subjected to lower temperatures and was not in direct contact with heat. In the microstructural examination of turbine components such as blades and vanes, regions such as the root and areas experiencing lower stress and temperature-like the bolt region in vanes- are commonly considered as reference points, representing microstructures similar to new, unexposed component (31). Figure 2(a) shows the metallographic image of that region after polishing without any etching. Blocky precipitates with morphologies consistent with MC carbides are clearly

observed on grain boundaries and within grains. Although optical microscopy primarily reveals morphological features, the blocky shape and distribution of these precipitates, combined with the known phase formation tendencies of nickel-based superalloys- where MC carbides are typically the first to from- strongly support their indentification as MC carbides. MC carbides are the primary solidification phase in such alloys and, due to hydrostatic tension from the surrounding melt during solidification, they exhibit diverse morphologies (20, 31). Similar observations of MC carbides morphology and distribution have been reported in previous studies, supporting our interpretation (20). Another prominent feature in this image is the grain boundaries that have not coarsened, where fine precipitates consistent with secondary $M_{23}C_6$ carbides appear discontinuously. optical microscopy reveals their morphology and distribution patterns, and their finer size and discontinuous presence on grain boundaries, along with the established metallurgy of nickel-based superalloys under prolonged elevated temperatures, strongly indicate their identity as $M_{23}C_6$ carbides. This observation aligns with previous findings indicating that such secondary carbides contribute to the material's high-temperature strength and reflect an absence of severe thermal exposure or microstructural degradation that could jeopardize the component's integrity (20). In Figure 2(b), besides the primary MC carbides, dense regions rich in γ' precipitates are visible. Given their fine size and high density, it can be inferred that this microstructural zone was not subjected to high-temperature fields capable of causing significant microstructural evolution. Figure 2(b) also highlights regions marked with a red circle containing dense, uncoarsened minute features (or fine, unresolved precipitates). Due to the resolution limits of optical microscopy, these appear as high-density areas; however, their precise morphology and phase cannot be conclusively identified at this magnification.

Figure 3a shows an unetched OM image of the service-exposed turbine vane region in the damaged area. This image reveals no voids or creep cavities, nor any cracks resulting from structural changes. However, a notable feature in Figure 3a is the increased volume fraction of carbides. Unlike gamma prime, which typically undergoes coarsening and/or dissolution during high-temperature service, the observed increase in the secondary $M_{23}C_6$ carbide volume fraction is attributed to thermal exposure promoting their precipitation, consumption of matrix elements for their formation, or perhaps slight carburization, if applicable. This change in carbide distribution and quantity can significantly influence grain boundary integrity or overall mechanical properties. Figure 3a clearly illustrates an increased volume fraction of secondary $M_{23}C_6$ carbides. This observation is made by direct comparison with the microstructure of the reference sample (Figure 2a), which represents the as-received state or less thermally affected region of the material. The elevated temperature exposure during service has evidently promoted further precipitation of these carbides. Carbides are coalescing along interdendritic regions and approaching each other. Typically, the volume fraction of secondary carbides increases due to long-term aging or service conditions. Under these conditions, with high temperature and applied stresses, diffusion finds favorable conditions. Under these circumstances. MC carbides, which are the primary source of carbon in the structure, begin to dissolve according to reaction 1 and form $M_{23}C_6$ carbides, stabilizing them. In this case, microstructural observations (Figures 2a and 3a) suggest a transformation process where chromium, molybdenum, and tungsten may react with carbon to form complex chromium-based carbides. This is consistent with the widely reported reaction in the literature for such alloys (20, 31):

$$MC + \gamma = M_{23}C_6 + (MC)_{Transformed} \quad (1)$$

In fact, by consuming carbon and γ, the volume fraction of secondary precipitate phases will increase. With the decomposition of the primary MC carbide, titanium and niobium present in the structure are released (32). The released carbon combines with chromium to form complex $M_{23}C_6$ carbides. With the depletion of chromium from the γ matrix, γ becomes unstable, and conditions are created for nickel to participate in the formation of γ'. (32). The titanium released from MC reacts with nickel in the matrix to form Ni3Ti (32). As this process continues, if Al is released from the γ matrix, a complex γ' phase is formed. Otherwise, the formation of a blocky η phase is possible. The overall description of this issue can be summarized in reaction 2 (31).

$$MC + \gamma = M_{23}C_6 + \gamma' \quad (2)$$

The coarsening of carbides and their coalescence to form a carbide film, along with the growth of γ' precipitates, can be seen in Figure 3b. Along the grain boundaries of the carbides, a eutectic carbide structure is evident. The presence of hafnium and tungsten usually stabilizes eutectic structures, which limit and reduce the dissolution temperature (33). Since eutectic phases are the last phases

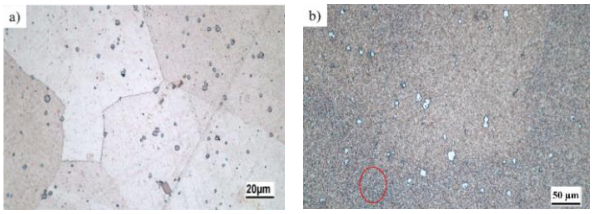

Figure 2. OM images of the low-damage region of the vane in this study: (a) high magnification; and (b) low magnification

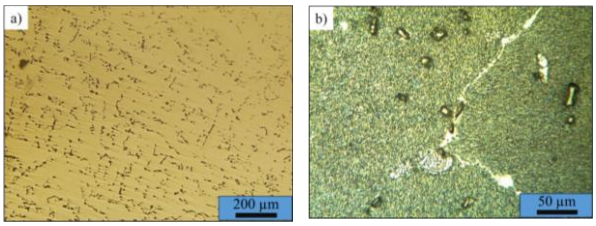

Figure 3. OM images of the high-damage region of the vane in this study: (a) low magnification; and (b) high magnification

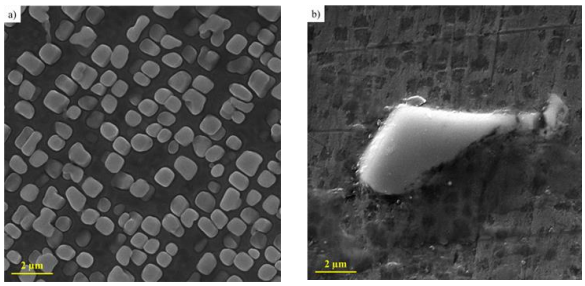

Figure 4. FESEM images of the Next- Generation Nickel Superalloy microstructure: (a) reference sample, and (b) service exposed vane

to form during solidification, they are the first to dissolve and, due to their presence, the dissolution temperature cannot be significantly increased as it would lead to local melting and structural damage (34, 35).

Figure 4 presents FESEM images of the investigated nickel-based superalloy in both the reference sample and service-exposed conditions, providing insight into the microstructural evolution under operational stresses. In Figure 4(a), the image of the reference sample after electropolishing is shown. Electropolishing enhances the surface morphology by selectively removing material and revealing precipitate shapes more clearly, allowing the observation of cubic γ' precipitates characteristic of a virgin microstructure. These cubic γ' precipitates are well-known as the primary strengthening phase in nickel-based superalloys and their morphology, size, and distribution critically influence the mechanical properties, especially at elevated temperatures (34, 36). The clear visualization of these cubic γ' precipitates in the FESEM image confirms the successful preservation of the initial heat-treated microstructure in the reference sample. Figure 4(b) presents the FESEM image of the nickel superalloy after 1200 service cycles, taken from the mid-span region of the 2nd stage vane. This image was intentionally obtained without electropolishing in order to capture the surface morphology and real operational microstructural state, including possible surface degradation, oxidation, or precipitate evolution under service conditions. Such an approach allows the investigation of γ' precipitate coarsening, morphological changes, and potential formation of secondary phases in a state representative of actual turbine service (35). It is important to note that surface etching was performed in separate samples to quantitatively assess the volume fraction of γ' precipitates, as etching enhances contrast between the matrix and precipitates. Typically, in the micrographs of the reference sample, a bimodal distribution of γ' precipitates is observed: primary cubic γ' precipitates, which tend to coarsen and slightly change morphology after aging, and secondary, nano-sized spherical γ' precipitates formed during prolonged aging. The primary precipitates are clearly visible even at moderate magnifications in FESEM images (34, 36), while the secondary precipitates, due to their nanoscale dimensions, are discernible only at higher magnifications or using advanced characterization techniques such as FESEM. This bimodal γ' microstructure is essential for balancing strength and creep resistance in service conditions. In contrast, the investigated superalloy in this study exhibits a predominantly mono-phase and uniform γ' precipitate structure in the reference condition, which might reflect specific heat treatment parameters or alloy composition aimed at optimizing service performance. Such a uniform γ' distribution can also influence the hardness and creep properties, as finer and more uniform precipitates generally improve high-temperature mechanical behavior (34, 36).

Table 2 presents the statistical results of the structural analysis of γ' precipitates. As can be seen, the volume fraction of γ' precipitates has increased by 5 %, and their average size has increased by approximately 230 nm after service. The small change in volume fraction and the 40 % increase in precipitate size indicate that the component was subjected to high temperature and low stress fields. This is consistent with the fact that the reference sample is a vane and operates stationarily in the turbine, so it is naturally subjected to low stress, and the damage caused by high temperature is more significant. . Another point that can be inferred is that, despite the observed changes in the ´γ precipitate content and size, the alloy maintained structural integrity under these service conditions for 1200 cycles, suggesting a degree of physical stability within the operational limits, even with microstructural evolution.

Figure 5 presents FESEM images of the MC carbide-containing region in the Service-exposed vane after operational use, captured in both backscattered electron

TABLE 2. Statistical results of the analysis of γ' precipitate characteristics in reference and service exposed vane

Sample Condition	Volume Fraction of ´γ (%)	Average size of ´γ(nm)
Reference sample	43.72	530 ± 15
Service Exposed Vane	48.86	763 ± 15

(BSE) mode (right) and secondary electron (SE) mode (left), accompanied by the elemental distribution map of the same area. These imaging techniques provide complementary insights, with BSE highlighting compositional contrasts and SE revealing surface morphology, thereby enabling a comprehensive microstructural characterization of the carbide phases and their surroundings. Although precise nanoscale modifications and subtle morphological deviations of the γ' precipitates (approximately 0.7 µm in size) remain challenging to resolve fully at this magnification scale (10 µm scale bar), a qualitative trend of γ' coarsening is evident. Notably, there is a discernible morphological transition from the initial well-defined cubic shape toward a more spheroidal form. This observation aligns with prior studies documenting γ' phase coarsening as a common microstructural evolution under prolonged high-temperature service conditions, which significantly influences mechanical properties such as creep resistance (37). The elemental distribution map further reveals significant enrichment of Ti and C within the carbide-rich regions, confirming the presence and remarkable stability of TiC carbides after 1200 service cycles. This finding corroborates earlier reports indicating that TiC carbides exhibit strong thermal stability, which plays a critical role in maintaining microstructural integrity during high-temperature exposure (37, 38). The formation and growth of $M_{23}C_6$ carbides in this nickel-based superalloy are typically linked to the partial decomposition of primary MC carbides. During service, constituent elements initially stabilizing MC carbides—often Nb and Ta rather than Ti—are released into the matrix upon decomposition, providing the requisite elements for the nucleation and subsequent growth of $M_{23}C_6$ carbides. Existing literature suggests two primary transformation pathways: direct conversion of MC carbides to $M_{23}C_6$ or a two-step transformation via an unstable M6C intermediate phase before stabilizing as $M_{23}C_6$ (37). Importantly, the stability of these carbides, attributed to their preferential localization at interdendritic sites, impedes grain boundary migration, thereby enhancing creep resistance and overall mechanical stability during high-temperature service (38). To quantitatively evaluate the chemical stability and elemental distribution within the carbides and their adjacent regions, EDS analysis was conducted on selected areas marked in Figure 5. This analysis confirms the compositional variations consistent with the aforementioned transformation mechanisms and phase stability, thereby providing a more comprehensive understanding of microstructural evolution in service-exposed nickel superalloys.

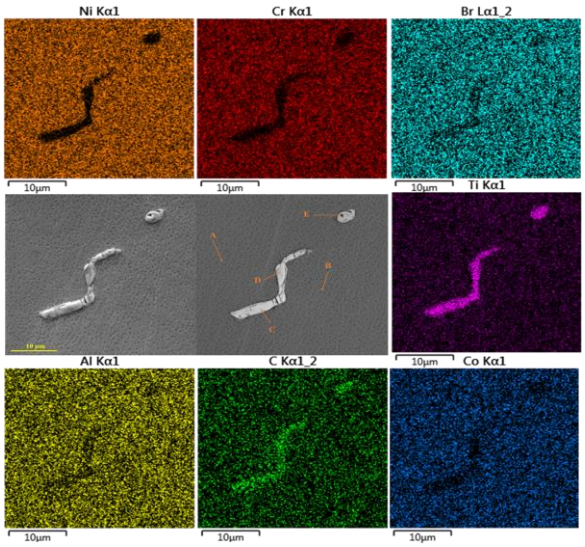

Figure 5. FESEM image in both BSE and SE modes along with an elemental map of the region

Based on the elemental maps, except for C and Ti which are highly concentrated in the M(Ti)C region, the remaining elements are well-distributed within the γ matrix. The Al elemental map clearly shows the enrichment of this element in certain regions, attributable to the growth and coarsening of γ' precipitates. Figure 6a presents the EDS spectrum and results for region A in Figure 5. The EDS results for this region confirm that it is the γ phase. The presence of Ti and Al in the analysis results for this region is due to the larger EDS analysis window compared to the region of interest, which includes contributions from the surrounding γ' precipitates. These observations also hold true for region B in Figure 5, which is also the γ matrix phase. For region C, based on the EDS results, it can be concluded that this carbide is of the MC type, given the absence of Cr, and is stabilized by Nb, Ti, W, and Ta. The EDS results for region D, which is another part of the same carbide, are very similar. Typically, during service, MC carbides undergo compositional changes, either directly or through intermediate phases like M6C, before transforming into $M_{23}C_6$. However, the observed stability in various regions of the carbide indicates that the carbide in question has not yet entered the dissolution stage. This supports the previous claim regarding the stability of TiC carbides. The EDS results for region E, as shown in Figure 6e, also confirms the presence of MC carbide stabilized by Nb, Ti, W, and Ta.

The XRD and Rietveld analysis results in Figure 7 reveal a significant increase in the gamma prime phase content of the in-service vane compared to the reference sample. This increase can be attributed to the structural and thermodynamic changes occurring in the investigated nickel superalloy during service. Thermodynamic laws support these changes. The increase in gamma prime and intermetallic phases signifies a decrease in the system's degrees of freedom (F), as predicted by the Gibbs phase rule. As the number of phases (P) increases, the system moves toward a new equilibrium state with greater stability.

$$F = C - P + 2 \quad (3)$$

Furthermore, the Gibbs-Helmholtz equation indicates that with increasing temperature and entropy during service, the Gibbs free energy (ΔG) decreases. A decrease in ΔG favors the formation of new and more stable phases, including the gamma prime phase.

$$\Delta G = \Delta H - T\Delta S \quad (4)$$

$$T\,\Delta S > \Delta H \quad (5)$$

$$\Delta G < 0 \quad (6)$$

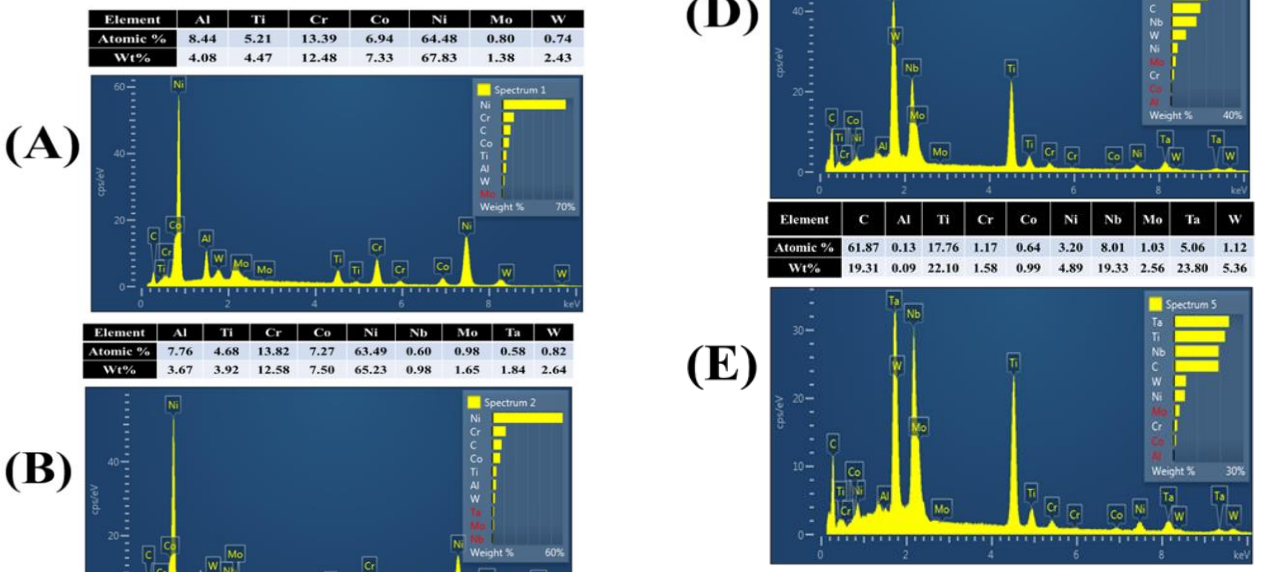

Figure 6. EDS results of the marked regions in the FESEM image (Figure 5): (a) Region A, (b) Region B, (c) Region C, (d) Region D, and (e) Region E

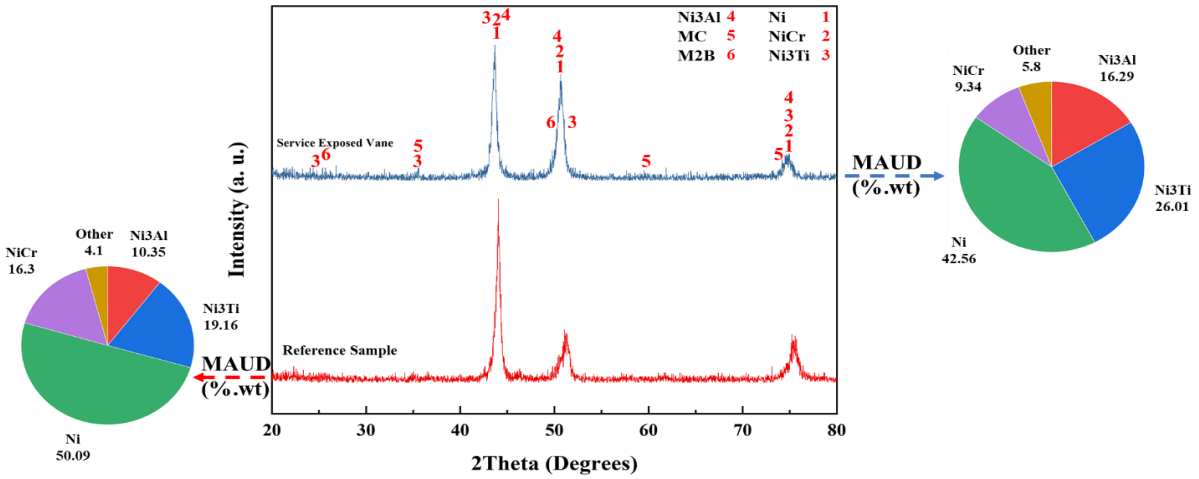

Figure 7. XRD and Rietveld analysis results of reference sample and service exposed vane

Rietveld results also confirm these findings, indicating significant microstructural evolution during service. Specifically, the gamma phase decreased from 66.39 to 51.90 wt%, while the gamma prime phase increased from 29.51 to 42.30 wt%. This observed increase in the gamma prime phase content in the in-service vane, while less common than coarsening, suggests that under these specific service conditions thermal cycles, there might be a driving force for additional precipitation from the supersaturated gamma matrix. This phenomenon, which represents a combination of continued precipitation and subsequent grain growth mechanisms during service, is influenced by various factors such as internal stresses due to temperature changes, the presence of alloying elements, and atomic diffusion within the crystal lattice. A comparison of the calculated lattice parameters for the gamma' phase also indicates a slight lattice expansion and the possibility of crystal defects in this phase. These substantial changes in the microstructure directly affect the mechanical properties of the vane, leading to reduced strength and increased creep.

Figure 8 presents a schematic of the γ' precipitate growth mechanism. The corners of cubic γ' precipitates are more susceptible to diffusion due to lattice mismatch and the localized increase in surface energy. This phenomenon, which is well-documented in the literature, causes atoms to diffuse from the high-energy corners to the lower-energy interfaces, causing the precipitates to gradually become quasi-spherical (39). As the morphology of the γ' precipitates approaches a quasi-spherical shape, external stress influences their preferential growth, a key characteristic of stress-induced directional coarsening, or rafting. This growth typically occurs perpendicular to the applied tensile stress direction, as the elastic strain energy is minimized by this specific orientation (40). Subsequently, the precipitates coarsen and preferentially become elliptical, marking the beginning of the rafting stage. The formation of these aligned γ' rafts leads to a significant decrease in the overall high-temperature mechanical properties and creep resistance of the superalloy (41). This behavior is attributed to the reduced interface area between the γ and γ' phases and the formation of continuous γ channels, which facilitate dislocation motion and bypass mechanisms. Our observations of γ' precipitate growth and rafting are consistent with the findings of other researchers who have studied the microstructural evolution of nickel-based superalloys under similar thermo-mechanical conditions (42, 43). The transition from a stable cubic morphology to a rafted structure is a crucial degradation mechanism in these alloys, directly impacting their service life. This highlights the importance of microstructural stability in maintaining the long-term performance of components exposed to high temperatures and mechanical loads.

The solidification sequence of next-generation nickel superalloy was determined experimentally and is observed to be as follows:

$$L \rightarrow L + MC \rightarrow L + MC + \gamma \rightarrow L + MC + \gamma + \gamma' \quad (7)$$

This sequence was primarily established through DSC conducted on the as-cast samples, complemented by microstructural examination of the solidified structure. To determine the initial melting temperatures of the various phases, DSC heating curves were obtained for both reference sample and service-exposed vanes (Figure 9). Results indicate that the initial melting temperatures of the γ + γ', γ + MC, and γ matrix phases did not exhibit significant changes between the reference sample and service-exposed vanes, which is consistent with FESEM results. It is important to note that for typical nickel-based superalloys, the gamma matrix generally has a melting point in the range of approximately 1350-1450 ºC, while the gamma' phase has a solvus temperature (dissolution temperature) typically ranging from 1100-1250 ºC, and its full melting occurs at higher temperatures, often very close to or overlapping with the gamma phase melting point, depending on composition. The observed increase in the overall melting temperature in the service-exposed vane indicates a shift in the thermodynamic equilibrium of the system. This shift in equilibrium can be attributed to the significant increase in the gamma' phase content during service, which alters the average composition and phase balance, thereby affecting the solidus/liquidus temperatures of the bulk

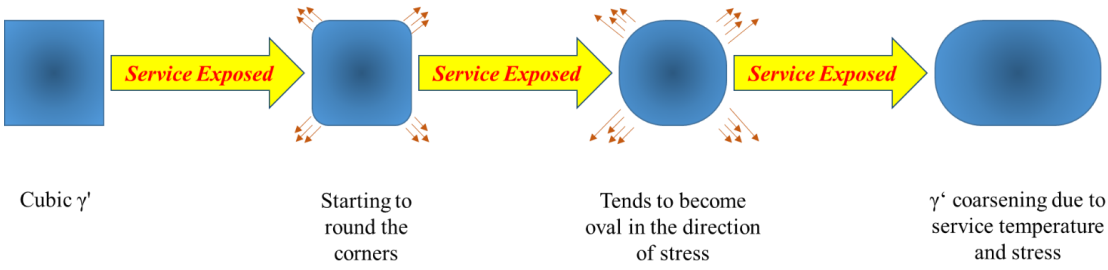

Figure 8. Mechanism of morphology change and growth of γ' precipitates during service

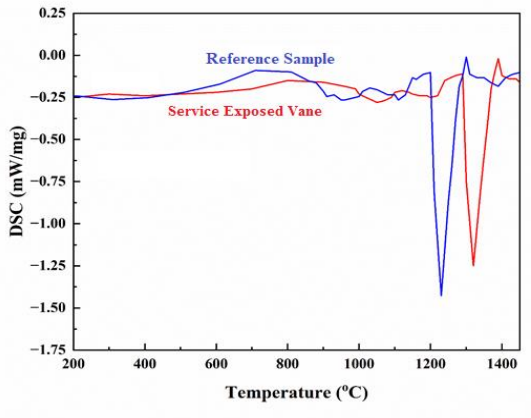

Figure 9. DSC analysis results of reference sample and service exposed vanes

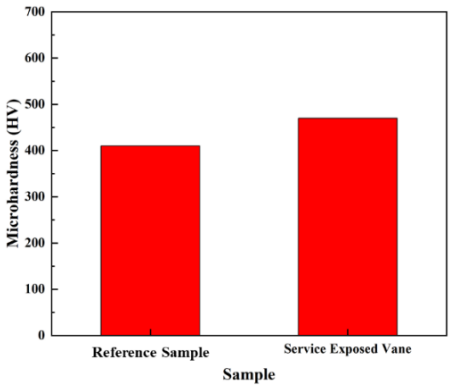

Figure 10. Hardness change in reference sample and service exposed vanes

material. Also, the increase in melting temperature in the service-exposed vane indicates a shift in the thermodynamic equilibrium of the system. This shift in equilibrium can be attributed to the significant increase in the γ' phase (20, 32). The formation and growth of the γ' phase lead to a decrease in the Gibbs free energy of the system, establishing a new equilibrium state. The thermodynamic mechanisms governing this process include a reduction in interfacial energy between different phases and a decrease in strain energy due to accommodating lattice mismatches (32, 34). It is important to note that these temperatures may exhibit some acceptable deviations due to the influence of thermal history. The DSC thermal lag, which is a constant independent of heating rate, can also affect the measured onset temperature of the melting peaks. Additionally, the models used in these studies tend to underestimate the experimental values.

Figure 10 presents the hardness results of reference sample and service-exposed vane, elucidating the hardness changes during service. As observed, the hardness exhibited an approximate increase of 60 Vickers, primarily attributed to the growth of gamma prime precipitates, their coalescence, and the formation of $M_{23}C_6$ carbide films. The coarsening of secondary precipitates led to the formation and strengthening of barriers against dislocation motion. The creation of these barriers and the subsequent restriction of dislocation movement hindered plastic deformation during the hardness test, a phenomenon previously reported in the literature (32). Plastic deformation during static loading in hardness testing is suppressed. While detrimental TCP phases such as sigma and mu phases are reported in the literature to affect hardness, in the current study these phases were not clearly detected by XRD or FESEM/EDS, likely due to their very low volume fraction. Therefore, the observed hardness increase is primarily attributed to the growth and coalescence of gamma prime precipitates and the formation of $M_{23}C_6$ carbide films. These phases create significant obstacles to dislocation motion, contributing to increased hardness. The trapping of dislocations behind these obstacles resulted in increased hardness. Additionally, the high density of secondary phases increased the anti-phase boundary content, contributing to the overall hardness increase (44). This change in hardness led to a compromise in creep resistance and overall component performance. During high-temperature operation, a constant interplay between hardening and softening governs the creep life of the component. Excessive softening, due to plastic deformation, elongation, and severe contact with opposing equipment, can lead to catastrophic failure. On the other hand, excessive hardening can render the component unable to withstand stress, resulting in brittle fracture (44-46). Therefore, both reference sample and service-exposed vanes were subjected to creep tests.

Figure 11 presents the creep test results for both the reference sample and service-exposed vane. Notably, the service-exposed vane exhibited a rapid and brittle failure compared to the reference sample. In the creep curve of the reference sample, all three creep regions are observable, whereas only regions 1 and 2 are evident in the service-exposed vane. The absence of the tertiary creep region in the service-exposed vane is a direct consequence of its brittle failure, which occurs without any significant necking. This behavior is attributed to the extensive microstructural changes that occurred during service, particularly the growth of gamma prime precipitates and the formation of continuous carbide films at grain boundaries. These microstructural changes significantly alter the deformation mechanism. The formation of carbide films, in particular, renders grain boundary sliding extremely difficult, if not impossible.

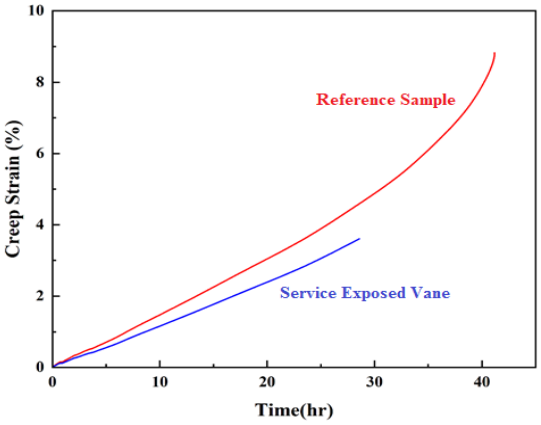

(a)

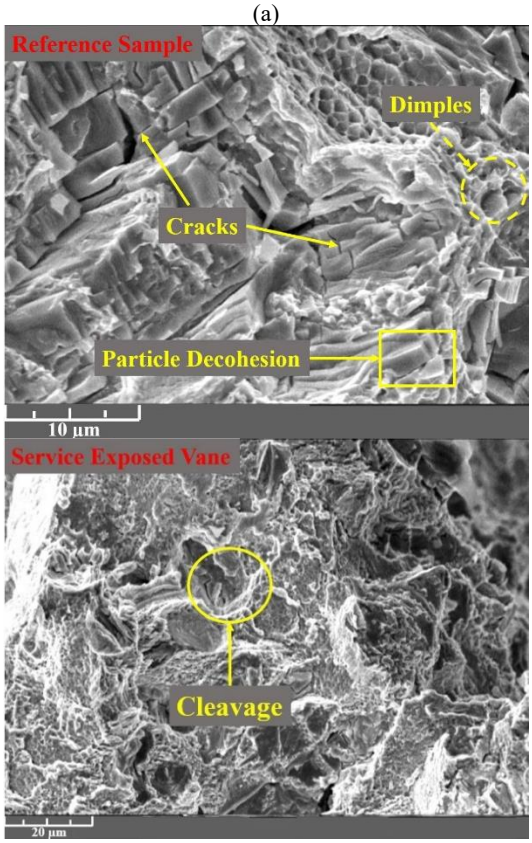

(b)

Figure 11. (a) Variation of creep properties, and (b) SEM images of the fracture surfaces of the reference sample and service-exposed vanes

The resistance created against sliding induces a shift in the deformation mechanism, a phenomenon well-documented in the literature (47, 48). Consequently, creep cavities form and coalesce at grain boundaries, leading to crack initiation. The rapid propagation of these cracks under high stress and temperature conditions results in the observed swift failure. Additionally, the formation of other cracks within the dendritic regions due to the interaction and shearing of dislocations and obstacles, as reported by other researchers (48, 49), further accelerates the failure process. The presence of a tertiary creep region in the reference sample, however, indicates a classic interplay between softening and hardening mechanisms, leading to a much longer creep life. This is consistent with findings in other studies on similar alloys (50). Furthermore, based on the SEM images, the reference sample exhibits numerous dimples indicative of ductile failure, characterized by significant energy absorption. This ductile failure is attributed to the nucleation, growth, and coalescence of creep cavities, which is consistent with stable crack propagation. The presence of these dimples and the distinct ductile fracture morphology confirm a more gradual failure process, with cracks propagating predominantly through the gamma matrix in a relatively dispersed manner. In contrast, the SEM images of the service-exposed vane reveal cleavage facets, which are typical of brittle failure and associated with rapid crack propagation and low energy absorption. This brittle behavior is consistent with both the absence of significant necking in the creep curve and the lack of a tertiary creep region, as previously discussed. This observed shift from a ductile to a brittle failure mechanism is a critical finding that is well-aligned with the documented effects of long-term thermal exposure on nickel-based superalloys (49, 50). The formation and growth of gamma prime precipitates and the development of carbide films at grain boundaries contribute significantly to the observed creep resistance but also promote brittleness by inhibiting grain boundary sliding. This microstructural evolution is confirmed as the key factor underlying the shift from ductile to brittle failure in the service-exposed vane.

As illustrated in Figure 11, the reference sample exhibited a creep life of 40 hours and a creep strain of 9%. In contrast, the service exposed vane, due to degradation mechanisms, displayed a significantly shorter creep life of 29 hours and a creep strain of only 4%. This substantial reduction in creep life clearly highlights the impact of degradation mechanisms on the material's properties.

4. CONCLUSIONS

This study focused on the independent effects of direct gas heat exposure on the microstructure, mechanical properties and creep behavior of the Next- Generation turbine Nickel Superalloy after 1200 cycles of operation. The following results were obtained:

1. Rietveld refinement was applied and the calculation indicated that the gamma prime phase increased from 29.51 to 42.30 wt.%, signifying precipitation and grain growth mechanisms during service.
2. An increase in the volume fraction of carbides and the growth of γ' precipitates were observed in the

superalloy microstructure after 1200 cycles of operation.

3. The hardness of the superalloy increased from 420 Vickers for the reference sample to 480 Vickers for the service exposed vane after 1200 cycles of operation.
4. Thermal analysis revealed a significant 60°C decrease in the complete dissolution temperature after service exposure, indicating a reduction in the alloy's overall thermal stability and suggesting the need for repair or rejuvenation. However, the onset melting temperatures of key phases remain largely unchanged, reflecting stable initial melting behavior under service conditions.
5. The creep strain rate of the superalloy decreased after 1200 cycles of operation.

5. REFERENCES

1. Koç Ö, Thomas R, Liang X, Hegedues Z, Lienert U, Harrison RW, et al. A spatially resolved analysis of dislocation loop and nanohardness evolution in proton irradiated Zircaloys. Acta Materialia. 2024;269:119799. https://doi.org/10.1016/j.actamat.2024.119799
2. Sujata M, Madan M, Raghavendra K, Venkataswamy M, Bhaumik S. Identification of failure mechanisms in nickel base superalloy turbine blades through microstructural study. Engineering Failure Analysis. 2010;17(6):1436-46. https://doi.org/10.1016/j.engfailanal.2010.05.004
3. Golezani A, Bageri M, Samadi R. Microstructural change and impact toughness property of Inconel 738LC after 12years of service. Engineering Failure Analysis. 2016;59:624-9. https://doi.org/10.1016/j.engfailanal.2015.11.012
4. Kumawat MK, Parlikar C, Alam MZ, Das DK. Type-I hot corrosion of Ni-base superalloy CM247LC in presence of molten Na2SO4 film. Metallurgical and Materials Transactions A. 2021;52(1):378-93. https://doi.org/10.1007/s11661-020-06068-6
5. Antolovich SD. Microstructural aspects of fatigue in Ni-base superalloys. Philosophical Transactions of the Royal Society A: Mathematical, Physical and Engineering Sciences. 2015;373(2038):20140128. https:// doi.org/10.1098/rsta.2014.0128
6. Shajari Y, Seyedraoufi Z, Alizadeh A, Razavi S, Porhonar M, Mirzavand K. Effect of solution temperature of rejuvenation heat treatment on the stability of γ′ precipitates in Ni-base superalloy IN738LC during long-term heating. Materials Research Express. 2019;6(12):126571. https://doi.org/10.1088/2053-1591/ ab54ef
7. Belan J, editor Quantitative evaluation of alitize coating on ŽS6K Ni-base superalloy. Materials science forum; 2014: Trans Tech Publ.
8. Belan J, Vaško A, Kuchariková L, Tillová E, Chalupová M. The SEM Metallography analysis of vacuum cast ZhS6K superalloy turbine blade after various working hours. Manufacturing Technology. 2019;19(5):727-33. 10.21062/ujep/362.2019/a/12132489/MT/19/5/727
9. Belan J, Klacková M. Structure and Its Influence on Ni–Base Superalloy Mechanical Properties. 2013. https://depot.ceon.pl/handle/123456789/3515
10. Kawagishi K, Yeh A-C, Yokokawa T, Kobayashi T, Koizumi Y, Harada H. Development of an oxidation-resistant high-strength sixth-generation single-crystal superalloy TMS-238. Superalloys. 2012;9:189-95. https://doi.org/10.1002/9781118516430.ch21
11. Tyagunov A, Baryshev E, Kostina T, Baum BA, Lesnikov V, Semenova IP. The Effect of Long-Term High-Temperature Heat Treatment at 950 C on the Structure and Mechanical Properties of the ZhS6U Superalloy. PHYSICS OF METALS AND METALLOGRAPHY C/C OF FIZIKA METALLOV I METALLOVEDENIE. 1998;86:65-9.
12. Tewari S, Hemareddy M. Soviet superalloy ZHS6-K, effect of B/C modification. Journal of Materials Science. 1983;18(4):1155-64. https://doi.org/10.1007/BF00551985
13. Du B, Sheng L, Cui C, Hu Z, Sun X. Effects of grain refinement on the low-cycle fatigue behavior of IN792 superalloys. Crystals. 2021;11(8):892. https://doi.org/10.3390/cryst11080892
14. Wei T, Ding K, Wu G, Liu X, Fan M, Zhang Y, et al. Stress rupture initiated by the carbides in the grain boundaries of the multi-pass weld metal. Journal of Materials Research and Technology. 2021;10:282-90. https://doi.org/10.1016/j.jmrt.2020.12.031
15. Taheri M, Jam JE, Beni MH, Khorram A, Kashani-Bozorg SF, Torkamany MJ. The effect of service temperature on the impact strength and fracture toughness of GTD-111 superalloy. Engineering Failure Analysis. 2021;127:105507. https://doi.org/10.1016/j.engfailanal.2021.105507
16. Bi Z-n, Dong J-x, Zhang M-c, Zheng L, Xie X-s. Mechanism of α-Cr precipitation and crystallographic relationships between α-Cr and δ phases in Inconel 718 alloy after long-time thermal exposure. International Journal of Minerals, Metallurgy, and Materials. 2010;17(3):312-7. https://doi.org/10.1007/s12613-010-0310-z
17. Schlesinger M, Seifert T, Preussner J. Experimental investigation of the time and temperature dependent growth of fatigue cracks in Inconel 718 and mechanism based lifetime prediction. International Journal of Fatigue. 2017;99:242-9. https://doi.org/10.1016/j.ijfatigue.2016.12.015
18. Mahobia G, Paulose N, Mannan S, Sudhakar R, Chattopadhyay K, Srinivas NS, et al. Effect of hot corrosion on low cycle fatigue behavior of superalloy IN718. International Journal of Fatigue. 2014;59:272-81.
19. Lewis D, Ding R, Whittaker M, Mignanelli P, Hardy M. The effect of oxidising thermal exposures on the fatigue properties of a polycrystalline powder metallurgy nickel-based superalloy. Materials & Design. 2020;189:108529. https://doi.org/10.1016/j.matdes.2020.108529
20. Shajari Y, Razavi SH, Seyedraoufi ZS, M. Samiee. The effect of time and temperature of solutionizing heat treatment on γ ′ characterization in a Ni-base superalloy. Metallography, Microstructure, and Analysis. 2021;10(4):441-7. https://doi.org/10.1007/s13632-021-00760-8
21. Long H, Bakhtiari SR, Liu Y, Mao S, Wei H, Chen Y, et al. A comparative study of rafting mechanisms of Ni-based single crystal superalloys. Materials & Design. 2020;196:109097. https://doi.org/10.1016/j.matdes.2020.109097
22. Yu Z, Wang X, Yang F, Yue Z, Li JC. Review of γ'rafting behavior in nickel-based superalloys: crystal plasticity and phase-field simulation. Crystals. 2020;10(12):1095. https://doi.org/10.3390/cryst10121095
23. Tsukada Y, Murata Y, Koyama T, Miura N, Kondo Y. Creep deformation and rafting in nickel-based superalloys simulated by the phase-field method using classical flow and creep theories. Acta Materialia. 2011;59(16):6378-86. https://doi.org/10.1016/j.actamat.2011.06.050
24. Hosseini S, Nategh S, Ekrami A. Changes of γ′ precipitate characteristics in damaged superalloy IN738LC during different stages of rejuvenation heat treatment cycles. Materials Science

and Technology. 2012;28(2):213-9. https://doi.org/10.1179/1743284711Y.0000000021

25. Hosseini SS, Nategh S, Ekrami A-A. Microstructural evolution in damaged IN738LC alloy during various steps of rejuvenation heat treatments. Journal of alloys and compounds. 2012;512(1):340-50. https://doi.org/10.1016/j.jallcom.2011.09.094
26. Yang S, Yun J, Moon B, Park S, Seok C-S. Creep performance evaluation considering the operating environment of gas turbine blades with rejuvenation maintenance. Journal of Mechanical Science and Technology. 2022;36(1):127-34. https://doi.org/10.1007/s12206-021-1211-y
27. Azadian S, Wei L-Y, Warren R. Delta phase precipitation in Inconel 718. Materials characterization. 2004;53(1):7-16. https://doi.org/10.1016/j.matchar.2004.07.004
28. Simonetti M, Caron P. Role and behaviour of μ phase during deformation of a nickel-based single crystal superalloy. Materials Science and Engineering: A. 1998;254(1-2):1-12. https://doi.org/10.1016/S0921-5093(98)00766-7
29. De Luca A, Kenel C, Griffiths S, Joglekar SS, Leinenbach C, Dunand DC. Microstructure and defects in a Ni-Cr-Al-Ti γ/γ'model superalloy processed by laser powder bed fusion. Materials & Design. 2021;201:109531. https://doi.org/10.1016/j.matdes.2021.109531
30. Chengjian HBLHW. Solidification Microstructure of Ni-Base Superalloy Powder. Acta Metallurgica Sinica (English Letters). 1991;4(2):97.
31. Khodabakhshi A, Mashreghi A, Shajari Y, Razavi SH. Investigation of microstructure properties and quantitative metallography by different etchants in the service-exposed nickel-based superalloy turbine blade. Transactions of the Indian Institute of Metals. 2018;71(4):849-59. https://doi.org/10.1007/s12666-017-1217-4
32. Shajari Y, Beigi M, Porhonar M. The effect of microstructural changes on the rupture behavior of gas turbine damping bolt superalloy (Nimonic 90) after long service time. Engineering Failure Analysis. 2023;145:106993. https://doi.org/10.1016/j.engfailanal.2022.106993
33. D'Souza N, Kantor B, West G, Feitosa L, Dong H. Key aspects of carbide precipitation during solidification in the Ni-base superalloy, MAR M002. Journal of Alloys and Compounds. 2017;702:6-12. https://doi.org/10.1016/j.jallcom.2017.01.104
34. Shajari Y, Razavi SH, Seyedraoufi Z-S. Comparative study of solution heat treatment of IN738LC superalloy in conventional conditions and salt bath. Journal of Materials Engineering and Performance. 2022;31(3):2525-41. https://doi.org/10.1007/s11665-021-06344-5
35. Zhang H, Xie J, Li Q, Wu H, Yu J, Chai H, et al. Influence of Substituting W for Nb or Hf on Solidification Behavior of a Typical Co–Ni–Al–W Based Superalloy. Acta Metallurgica Sinica (English Letters). 2024;37(11):1907-20. https://doi.org/10.1007/s40195-024-01749-2
36. Bian H, Xu X, Li Y, Koizumi Y, Wang Z, Chen M, et al. Regulating the coarsening of the γ′ phase in superalloys. NPG Asia Materials. 2015;7(8):e212-e. https://doi.org/10.1038/am.2015.96
37. Zhang Z, Ding R, Guo Q, Liu C, Liu Y. Enhancing tensile and creep properties of Inconel 617 superalloy via regulating the synergistic evolution of M23C6 carbides and γ′ phases. Materials Science and Engineering: A. 2025;919:147523. https://doi.org/10.1016/j.msea.2024.147523
38. Singh Handa S. Precipitation of Carbides in a Ni-based Superalloy. 2014.
39. Moshtaghin R, Asgari S. Growth kinetics of γ′ precipitates in superalloy IN-738LC during long term aging. Materials & design. 2003;24(5):325-30. https://doi.org/10.1016/S0261-3069(03)00061-X
40. Hou J, Guo J. Influence of thermal exposure on the microstructures and mechanical properties of a superalloy. Journal of materials engineering and performance. 2006;15(1):67-75. https://doi.org/10.1361/105994906X83501
41. Wang Y, Li K, Cai Z, Shi L, Wang H. Creep behavior and microstructure evolution of Ni-based alloy IN617 at 1000° C. Materials Characterization. 2022;187:111837. https://doi.org/10.1016/j.matchar.2022.111837
42. Zhou Z, Lei Q, Zhang L, Cui Z, Shang Y, Qi H, et al. Microstructural evolution of nickel-based single crystal superalloy fabricated by directed energy deposition during heat treatment. Journal of Alloys and Compounds. 2022;904:163943. https://doi.org/10.1016/j.jallcom.2022.163943
43. Ping K, HUANG J-y, Feng L, HUANG L, Cui L. Mechanical properties and microstructural evolution of nickel-based superalloys. Transactions of Nonferrous Metals Society of China. 2025;35(7):2304-19. https://doi.org/10.1016/S1003-6326(25)66816-6
44. Sun F, Tong J, Feng Q, Zhang J. Microstructural evolution and deformation features in gas turbine blades operated in-service. Journal of alloys and compounds. 2015;618:728-33. https://doi.org/10.1016/j.jallcom.2014.08.246
45. Sun Z, Jiang X, Zhan X, Li K, Zheng W, Jiang D, et al. The recovery of microstructure and mechanical properties of directionally solidified Ni-based superalloy DZ411 after long-term thermal exposure at different temperatures. Materials Science and Engineering: A. 2023;888:145831. https://doi.org/10.1016/j.msea.2023.145831
46. Khodabakhshi A, Mashreghi A, Razavi S, Jafarpour S, Hajitaheri S, Shajari Y. Microstructure Characteristics of Rejuvenated Service Exposed Gas Turbine Blade under the Influence of Various Solution Temperature and Cooling Rates. Metallography, Microstructure, and Analysis. 2024;13(3):492-503. https://doi.org/10.1007/s13632-024-01093-y
47. Gai Y, Zhang R, Cui C, Zhou Z, Tao X, Tan Y, et al. Creep behavior and microstructure evolution of a novel Ni-Co-based superalloy with long-life designed for high temperature application. Materials Science and Engineering: A. 2025:148396. https://doi.org/10.1016/j.msea.2025.148396
48. Li Q, Tian S, Yu H, Tian N, Su Y, Li Y. Effects of carbides and its evolution on creep properties of a directionally solidified nickel-based superalloy. Materials Science and Engineering: A. 2015;633:20-7. https://doi.org/10.1016/j.msea.2015.02.056
49. Li K-S, Lu R-S, Gong X-F, Pei Y-B, Zhang X, Tan J-P, et al. Investigation of microstructural evolution and mechanical properties for in-service nickel-based superalloy. Materials Science and Engineering: A. 2024;899:146465. https://doi.org/10.1016/j.msea.2024.146465
50. Huang J, Ai C, Ru Y, Shang Y, Pei Y, Li S, et al. The Effect of Cooling Rate from Solution Treatment on γ′ Reprecipitates and Creep Behaviors of a Ni-Based Superalloy Single-Crystal Casting. Crystals. 2022;12(9):1235. https://doi.org/10.3390/cryst12091235

Persian Abstract

چکیده

در این پژوهش، تحول ریزساختاری و رفتار خزشی یک پره مرحله دوم توربین گاز پس از ۱۲۰۰ سیکل کارکرد طولانی‌مدت، از طریق بررسی‌های ریزساختاری و آزمون‌های خزشی مورد ارزیابی قرار گرفت. آنالیزهای میکروسکوپی افزایش در کسر حجمی و اندازه فازهای ثانویه نظیر گاما پریم و کاربیدها را آشکار ساخت. این تغییرات ریزساختاری منجر به تردی سوپرآلیاژ نیکل مورد بررسی گردید. نتایج آزمون سختی‌سنجی افزایش سختی از ٤٢٠ ویکرز برای پره نو به ٤٨٠ ویکرز برای پره تحت سرویس را نشان داد. آنالیز حرارتی کاهش ٦٠ درجه سانتیگرادی در دمای انحلال کامل را نمایان ساخت که حاکی از نیاز به تعمیر یا احیای آلیاژ می‌باشد. رشد رسوبات گاما پریم از طریق برش نابجایی‌ها و درشت‌شدن کاربیدها به دلیل ممانعت از لغزش مرزدانه‌ها، منجر به کاهش ۱۱ ساعته در عمر خزشی گردید. پره نو در تنش ۲٤۷ مگاپاسکال و دمای ۹۰۰ درجه سانتیگراد پس از ٤٠ ساعت با کرنش ۹٪ دچار شکست شد. در مقابل، پره تحت سرویس کاهش در عمر خزشی و کرنش خزشی را به ترتیب به ۲۹ ساعت و ٤٪ نشان داد.